ELSEVIER

Physics of the Earth and Planetary Interiors 126 (2001) 11–25

PHYSICS OF THE EARTH AND PLANETARY INTERIORS

www.elsevier.com/locate/pepi

An investigation of multi-domain hysteresis mechanisms using FORC diagrams

Christopher R. Pike [a], Andrew P. Roberts [b,*], Mark J. Dekkers [c], Kenneth L. Verosub [a]

[a] *Department of Geology, University of California, Davis, CA 95616, USA*
[b] *School of Ocean and Earth Science, Southampton Oceanography Centre, University of Southampton, European Way, Southampton SO14 3ZH, UK*
[c] *'Fort Hoofddijk' Paleomagnetic Laboratory, Faculty of Earth Sciences, University of Utrecht, Budapestlaan 17, 3584 CD Utrecht, The Netherlands*

Received 13 October 2000; received in revised form 26 April 2001; accepted 7 June 2001

Abstract

First-order reversal curve (FORC) diagrams provide a sensitive means of probing subtle variations in hysteresis behaviour, and can help advance our understanding of the mechanisms that give rise to hysteresis. In this paper, we use FORC diagrams to study hysteresis mechanisms in multi-domain (MD) particles. The classical domain wall (DW) pinning model due to Néel [Adv. Phys. 4 (1955) 191] is a phenomenological one-dimensional model in which a pinning function represents the interactions of a DW with the surrounding medium. Bertotti et al. [J. Appl. Phys. 85 (1999a) 4355] modelled this pinning function as a random Wiener–Lévy (WL) process, where particle boundaries are neglected. The results of Bertotti et al. [J. Appl. Phys. 85 (1999a) 4355] predict a FORC diagram that consists of perfectly vertical contours, where the FORC distribution decreases with increasing microcoercivity. This prediction is consistent with our experimental results for transformer steel and for annealed MD magnetite grains, but it is not consistent with results for our MD grains that have not been annealed. Here, we extend the DW pinning model to include particle boundaries and an Ornstein–Uhlenbeck (OU) random process, which is more realistic that a WL process. However, this does not help to account for the hysteresis behaviour of the unannealed MD grains. We conclude that MD hysteresis is more complicated than the physical picture provided by the classical one-dimensional pinning model. It is not known what physical mechanism is responsible for the breakdown of the classical DW pinning model, but possibilities include DW interactions, DW nucleation and annihilation, and DW curvature.

Keywords: First-order reversal curve (FORC); Domain wall (DW); Multi-domain (MD) particles

1. Introduction

Hysteresis in multi-domain (MD) systems is a complex phenomenon that involves domain wall (DW) nucleation and annihilation, DW pinning, and DW interactions. An understanding of MD hysteresis in its full range of behaviours is beyond present capabilities. For this reason, MD particle hysteresis has often been modelled in terms of DW pinning alone (e.g. Everitt, 1962; Schmidt, 1973; Dunlop and Xu, 1994; Bertotti, 1998), following the classical DW pinning model of Néel (1955). In this model, the complicated curvilinear pattern of DWs, as observed in real samples, is treated as a collection of non-interacting

* Corresponding author. Tel.: +44-1703-529011; fax: +44-1703-593059.
E-mail address: arob@mail.soc.soton.ac.uk (A.P. Roberts).

0031-9201/01/$ – see front matter
PII: S0031-9201(01)00241-2

planar DWs. Thus, a bulk sample is treated as if it were composed of small, non-interacting grains, each of which is a two-domain system with one planar DW. It is assumed that each DW travels through a one-dimensional DW pinning field, which represents the interactions of that DW with the surrounding material in a single grain. This pinning field can be modelled by a random function, and the behaviour of a bulk sample can be modelled by taking an average over an assemblage of grains (i.e. with a distribution of pinning fields). Clearly, this DW pinning model is overly simplistic and some studies have shown that it is inadequate for representing the natural MD samples encountered in paleomagnetism (Halgedahl and Fuller, 1983; McClelland and Sugiura, 1987; Shcherbakov et al., 1993). Nevertheless, this model has been widely used because it is difficult to devise a tractable model of MD hysteresis.

First-order reversal curve (FORC) diagrams (see below) provide a sensitive means of probing subtle variations in hysteresis behaviour. We have used FORC diagrams to investigate a wide range of magnetic particle systems (Pike et al., 1999, 2001; Pike and Fernandez, 1999; Roberts et al., 2000). In our previous work, we have adopted a combined experimental and theoretical approach in developing a framework for the interpretation of FORC diagrams. The agreement between experimental data and theory has demonstrated the usefulness of FORC diagrams as a means of investigating magnetic hysteresis in fine particle systems. In this paper, we extend our work with FORC diagrams to consider hysteresis mechanisms in MD particle systems. Following other workers (Néel, 1955; Dunlop and Xu, 1994; Dunlop and Özdemir, 1997; Bertotti, 1998; Bertotti et al., 1999a), we use the classical DW pinning model as a starting point and then compare this with experimental FORC diagrams for selected synthetic and natural MD samples.

2. FORC diagrams

A FORC diagram is calculated from a class of partial hysteresis curves known as FORCs (see Mayergoyz, 1986). As shown in Fig. 1, the measurement of a FORC begins by saturating a sample in a large positive applied field. The field is decreased to a reversal field H_a, and the FORC is the magnetization curve

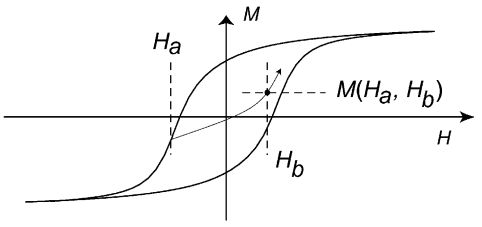

Fig. 1. Example of a major hysteresis loop with reversal point at H_a. FORC is the curve that starts at H_a and proceeds back to positive saturation. A magnetisation at an applied field H_b on the FORC with reversal field H_a is represented by $M(H_a, H_b)$.

that results when the applied field is increased from H_a back to saturation. By repeating this measurement for different values of H_a, one obtains a suite of curves such as those shown in Fig. 2(a). The magnetisation at the applied field H_b on the FORC with reversal field H_a is denoted by $M(H_a, H_b)$, where $H_b > H_a$ (Fig. 1). The FORC distribution is defined as the mixed second derivative:

$$\rho(H_a, H_b) \equiv -\frac{\partial^2 M(H_a, H_b)}{\partial H_a \partial H_b}, \quad (1)$$

where $\rho(H_a, H_b)$ is well defined for $H_b > H_a$. When a FORC distribution is plotted, it is convenient to change co-ordinates from $\{H_a, H_b\}$ to $\{H_c = (H_b - H_a)/2, H_u = (H_a + H_b)/2\}$. A FORC diagram is a contour plot of a FORC distribution with H_u and H_c on the vertical and horizontal axes, respectively (Fig. 2b). $H_b > H_a$, therefore $H_c > 0$, and a FORC diagram is confined to the right-hand half plane. The H_c co-ordinate is referred to as the microcoercivity.

To explain the motivation for calculating this mixed second derivative and for the change of co-ordinates, it is necessary to give a brief introduction to the Preisach model (Preisach, 1935). Let us begin by defining a simple mathematical construction, which is referred to as a hysteron. As shown in Fig. 3, the hysteron denoted by $\gamma_{\alpha\beta}$ equals 1 for large values of H; it switches to -1 when H is below H_α, and it remains at -1 until H passes H_β. When the second derivative in Eq. (1) is taken for the hysteresis behaviour of $\gamma_{\alpha\beta}$, the resulting $\rho(H_a, H_b)$ will have a peak at $H_a = H_\alpha$ and $H_b = H_\beta$, and will equal zero elsewhere, i.e. $\rho(H_a, H_b)$ will be a point delta function. In H_c and H_u co-ordinates, the FORC distribution $\rho(H_c, H_u)$ will consist of a point delta function at $H_c = (H_\beta - H_\alpha)/2$, $H_u = (H_\alpha + H_\beta)/2$. But $(H_\beta - H_\alpha)/2$

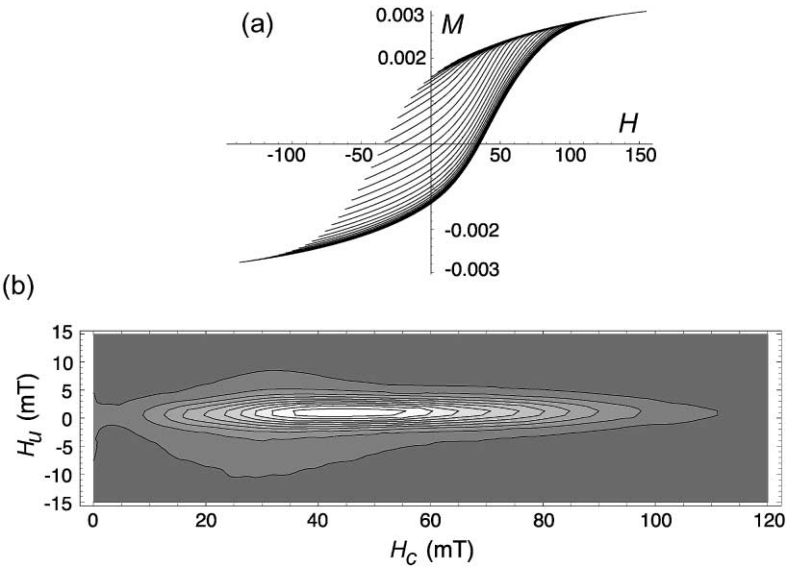

Fig. 2. (a) A set of 33 FORCs for sample CS911 from the Yucca Mountain ash flow tuff, from southern Nevada (see Eick and Schlinger, 1990; Worm, 1999). These FORCs are a subset of the 99 FORCs used for the following FORC diagram. Units used for M are Am^2 and mT for H. (i.e. Am^2 = the m is squared). (b) A FORC diagram for sample CS911, which indicates that the magnetic particles are in a non-interacting single domain state (SF = 2).

is the half-width of $\gamma_{\alpha\beta}$, which corresponds to its coercivity, and $(H_\alpha + H_\beta)/2$ is the horizontal offset of $\gamma_{\alpha\beta}$ which we refer to as its bias. Hence, on a FORC diagram, the H_c and H_u co-ordinates of the point delta function give the coercivity and bias, respectively, of this simple hysteron.

Similarly, for a collection of hysterons with a distribution of coercivities and biases denoted by

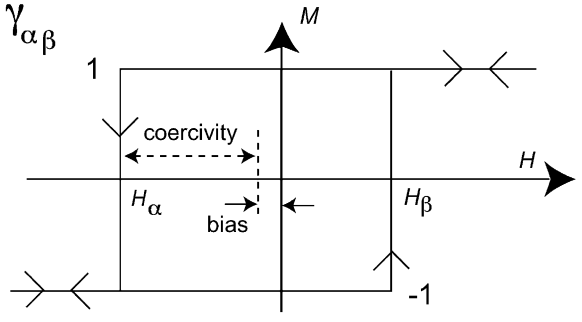

Fig. 3. The hysteron $\gamma_{\alpha\beta}$ equals 1 for large values of H, switches to -1 when H falls below H_α and remains at -1 until H rises above H_β. The half-width of the hysteron is its coercivity, and the horizontal offset of its centre is its bias.

$P(H_c, H_u)$, it can be shown that the FORC distribution $\rho(H_c, H_u)$ will be equivalent to $P(H_c, H_u)$. This type of mathematical hysteresis system, which consists of a collection of hysterons, is known as the Preisach model (Preisach, 1935), and the distribution of coercivities and biases, $P(H_c, H_u)$, is known as the Preisach distribution. In cases where a magnetic particle system can be rigorously represented by a collection of hysterons, the FORC and Preisach distributions will be equivalent.

The Preisach model of hysteresis was first suggested as a model of interacting single domain particles. In this model, each hysteron represents an individual particle in the assemblage. The coercivity of a hysteron corresponds to the coercivity of a single domain particle if it were magnetically isolated from other particles. The bias of a hysteron corresponds to a fixed interaction field, which represents the magnetostatic interaction of an individual particle with the surrounding assemblage of particles. The Preisach distribution therefore corresponds to the distribution of particle coercivities and interaction fields.

The original motivation in taking the second derivative in Eq. (1) was that, for single domain particle

systems, the FORC distribution $\rho(H_c, H_u)$ would be equivalent to the Preisach distribution, and to a distribution of particle switching and interaction fields. However, in practice, the hysteresis of an interacting single domain particle system is more complex and rich than can be described by a simple superposition of hysterons. Therefore, the Preisach model is only a phenomenological construction for modelling hysteresis in an approximate way, and the Preisach distribution is not a unique and well-defined quantity. In contrast to a Preisach distribution, the FORC distribution $\rho(H_c, H_u)$ is defined using only magnetisation data from FORCs, a second derivative, and a change of co-ordinates. Therefore, it remains a well-defined quantity regardless of whether a single domain particle system is consistent with the Preisach model. The FORC distribution is also a well-defined quantity for magnetic systems other than single domain particle assemblages, for which the Preisach model might have no apparent physical justification. We therefore distinguish a FORC distribution from a Preisach distribution. As shown below, FORC diagrams provide a useful empirical means of probing hysteresis behaviour.

Our FORC measurements were made using a Princeton Measurements Corporation alternating gradient magnetometer. The details of data acquisition and analysis involved in obtaining a FORC distribution have been described in detail elsewhere (Roberts et al., 2000). A certain amount of numerical smoothing is inherent in the calculation of a FORC diagram from experimental data: this is quantified by a smoothing factor (SF), which can vary between 2 for the highest quality data and 5 for poor quality data. In Fig. 2(b), we show the FORC diagram calculated (SF = 2) from the data in Fig. 2(a). The FORC distribution in Fig. 2(b) is narrowly confined to the centre horizontal axis, which is characteristic of a collection of non-interacting single domain particles. Magnetostatic interactions cause increased vertical spread of the contour loops about the peak (Pike et al., 1999; Roberts et al., 2000), while thermal relaxation of fine single domain particles shifts the FORC distribution to lower coercivities (Roberts et al., 2000; Pike et al., 2001). Before considering the manifestations of MD behaviour on FORC diagrams, it is instructive to consider the FORC diagrams expected for the classical DW pinning model of Néel (1955).

3. FORC diagrams and the classical DW pinning model

In the phenomenological DW pinning model of Néel (1955), a bulk sample is treated as an assemblage of small grains each of which contains one planar DW, where the DWs are completely non-interacting. Let us consider one such grain. For simplicity, let us assume that the DW passes through the cross-section of the grain which has cross-sectional area A and length L. Let us assume that the DW moves through a one-dimensional energy function, which takes into account all the interactions of that DW with the surrounding medium. Let us represent a grain by a line segment of length L, with end points at 0 and L. If the DW is located at x, then the magnetisation between 0 and x will be positive and the magnetisation between x and L will be negative. The total magnetic moment of the grain is: $M(x) = AM_s(L - 2x)$, where M_s is the spontaneous magnetisation per unit volume. Let us denote the energy of the DW as a function of position by $E_w(x)$. The demagnetisation field H_{de} will be approximated by the uniform field $-NM$, where N is the demagnetisation factor for this grain (rather than for the bulk sample) and M is the magnetic moment of the grain. The demagnetisation field in this grain is unaffected by the positions of the other DWs, as must be the case if the DWs are non-interacting. The demagnetisation energy E_{de} then becomes $\int_0^M -(\mu_0 H_{de})\,\mathrm{d}M = \int_0^M \mu_0 NM\,\mathrm{d}M = \mu_0 NM^2$. The total energy E_T will be the sum of E_w, E_{de} and the Zeeman energy $-\mu_0 MH$, where H is the applied field. So,

$$\begin{aligned} E_T(x, H) &= E_w(x) - \mu_0 M(x) H + \tfrac{1}{2}\mu_0 N M(x)^2 \\ &= E_w(x) - \mu_0 A M_s (L - 2x) H \\ &\quad + \tfrac{1}{2}\mu_0 N A^2 M_s^2 (L - 2x)^2. \end{aligned} \tag{2}$$

This expression has been used by Dunlop and Xu (1994) and others in studies of DW pinning.

The hysteresis of this model is governed by the requirement that the DW will always reside in a minimum of $E_T(x, H)$, with respect to x. As the applied field H is increased or decreased, the DW will move and follow the local energy minimum in which it resides. If the minimum in which it resides vanishes with changing H, then the DW will make a discontinuous

drop in energy to the next energy minimum of lower energy. This is a Barkhausen leap. Rather than working directly with $E_w(x, H)$, it is convenient to work with its gradient, which is referred to as the pinning field: $H_p(x) \equiv -(1/2\mu_0 AM_s)(dE_w(x, H)/dx)$. This pinning field is the critical input that governs the hysteresis behaviour of the model.

As discussed earlier, for systems that can be rigorously represented by a collection of hysterons, the FORC distribution and Preisach distributions will be equivalent. Bertotti et al. (1999a) showed that the above-described one-dimensional, non-interacting DW pinning model, after averaging over a distribution of pinning fields, can be rigorously described by a Preisach distribution. Hence, the FORC and Preisach models are equivalent in this case.

Néel (1955) modelled $H_p(x)$ as a collection of equispaced "saw-tooth" pinning sites, where the height of the "teeth" was a normally distributed random number. Néel (1955) investigated the Preisach (1935) distribution of this DW pinning model at low applied fields (i.e. the Rayleigh region) by neglecting the effects of demagnetisation energy. He found that the Preisach (and equivalently the FORC) distribution has a constant value near the origin. Bertotti et al. (1999a) and Magni et al. (1999) generalised $H_p(x)$ to a random Wiener–Lévy (WL) process, which is better known as Brownian motion in one dimension. In their mathematical treatment, these authors ignored the particle boundaries at $x = 0$ and L, and let x range over the real line. After averaging over a distribution of pinning fields, Bertotti et al. (1999a) obtained an analytical solution for the Preisach (and equivalently the FORC) distribution. Their result can be written as

$$M(H_a, H_b) = H_a\chi + \phi\chi + \left(\chi(H_b - H_a)\coth\left(\frac{(H_b - H_a)\chi}{\phi}\right) - 2\phi\chi\right), \tag{3}$$

where

$$\chi = \frac{1}{NAM_s^2} \quad \text{and} \quad \phi = \frac{\langle |dH_p|^2 \rangle}{2\,dx}.$$

This gives the Preisach or FORC distribution:

$$\rho(H_c) = \frac{2}{(\phi/\chi)^2}\frac{H_c\coth(H_c\chi/\phi) - 1}{\sinh^2(H_c\chi/\phi)}. \tag{4}$$

Hence, the Preisach (and equivalently the FORC) distribution is a decreasing function of H_c, and is independent of H_u; this implies that the FORC diagram for the DW pinning case will consist of vertical

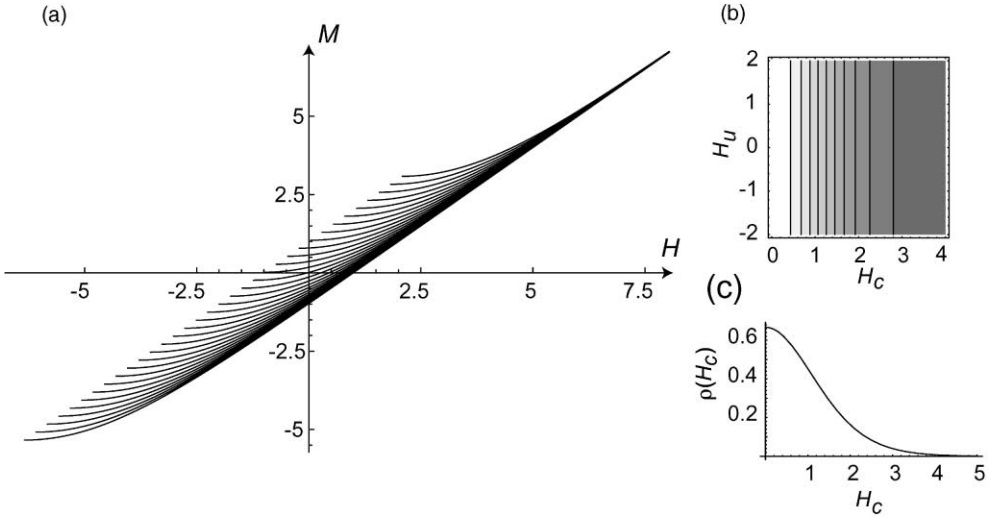

Fig. 4. Results for a distribution of one-dimensional, non-interacting DWs in a WL random process pinning field, from equations given by Bertotti et al. (1999a). (a) A set of FORCs calculated using Eq. (3) with $\chi, \phi = 1$. Note that since Bertotti et al. (1999a) neglected finite grain boundaries, these FORCs continue indefinitely in the upper right-hand quadrant with slope $\chi = 1$. (b) A FORC diagram, calculated using Eq. (4) and the same parameters as above, which consists entirely of vertical contours. (c) Cross-section of the FORC distribution in (b).

contours. To first order in H_c, the function in Eq. (4) has a constant value near $H_c = 0$, which is consistent with the result of Néel (1955). In Fig. 4, we show a set of FORCs generated using Eq. (3) with $\chi, \phi = 1$; we also show the resulting FORC distribution, and a cross-section of the FORC distribution at $H_u = 0$. Note that since Bertotti et al. (1999a) ignored particle boundaries, the FORCs in Fig. 4(a) will continue indefinitely into the upper right-hand quadrant, with slope $\chi = 1$. Later in this paper, we try to give the reader a more intuitive explanation for the predicted vertical contours on a FORC diagram.

4. Results — FORC diagrams for synthetic and natural MD samples

We have studied several MD materials in order to compare experimental results with theoretical predictions. M80 steel is an extremely soft magnetic material, with coercivity <1 mT. The magnetisation of the M80 sample is almost entirely reversible, and the irreversible signal is weak. It is therefore difficult to determine M_r/M_s for this sample. We have also investigated a limited range of natural MD particles, including a small hand-picked single grain of magnetite that was broken off a large crystalline sample which had crystal faces up to 20 mm across. The grain was equant and about 2 mm in size. We analysed this sample before and after annealing (before annealing $H_c = 7.5$ mT, $M_r/M_s = 0.078$; after annealing $H_c = 1.7$ mT, $M_r/M_s = 0.013$). The hysteresis loop measured before annealing is shown in Fig. 5(a); annealing substantially lowers the coercivity and remanence ratio. Annealing was achieved by heating the sample to 1200°C for 12 h in evacuated (10^{-6} mm Hg) quartz glass ampules. The furnace was then slowly cooled at 50°C steps, with a waiting time of 1 h at each step down to 500°C. The cooling rate was about 0.25–0.5°C/min. The furnace was then switched off and cooled slowly to room temperature over a 5 h period.

We also studied a smaller single grain of magnetite ($H_c = 1.9$ mT, $M_r/M_s = 0.019$), with dimensions of roughly 125 μm from the 150–100 μm fraction of sample HM4 (Fig. 5(b)), as studied by Hartstra (1982). Finally, we analysed a clay-rich late Pleistocene bulk sediment with abundant ice-rafted detritus from ocean drilling program (ODP) Hole 887B ($H_c = 5.9$ mT, $M_r/M_s = 0.056$) from the North Pacific Ocean (see Roberts et al., 1995, 2000).

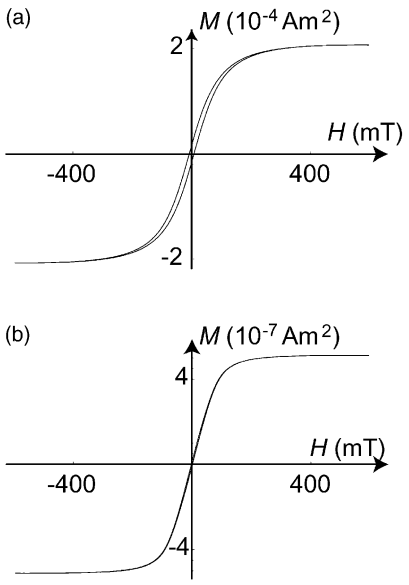

Fig. 5. Major hysteresis loops for two of the analysed samples: (a) a 2 mm magnetite grain before annealing; and (b) a 125 μm magnetite grain. On this scale, the loop in (b) appears to be closed. Hysteresis parameters for these samples are given in the text.

M80 transformer steel was selected as an example of classical DW pinning hysteresis. The weakness of the irreversible signal makes measurement of a FORC diagram difficult, however, using a 3 mm × 0.5 mm rectangular piece of M80, with the long direction parallel to the applied field, we acquired the FORC diagram shown in Fig. 6(a) (SF = 3). This diagram consists of vertical contour lines and a FORC distribution that decreases with increasing H_c. This behaviour is opposite to that of the horizontally elongated contour loops exhibited by the non-interacting single domain sample shown in Fig. 2(b).

FORC diagrams were acquired after and before annealing for the 2 mm magnetite sample (Fig. 6(b) and (c)). We also acquired a FORC diagram for the 125 μm magnetite from sample HM4 (Fig. 6(d)). In Fig. 7, we show a typical MD result from bulk sediment from ODP Hole 887B (see Roberts et al., 1995, 2000). We refer to this type of FORC distribution as a diverging contour pattern because the contours diverge from the $H_u = 0$ axis and intersect the $H_c = 0$ axis. Similar

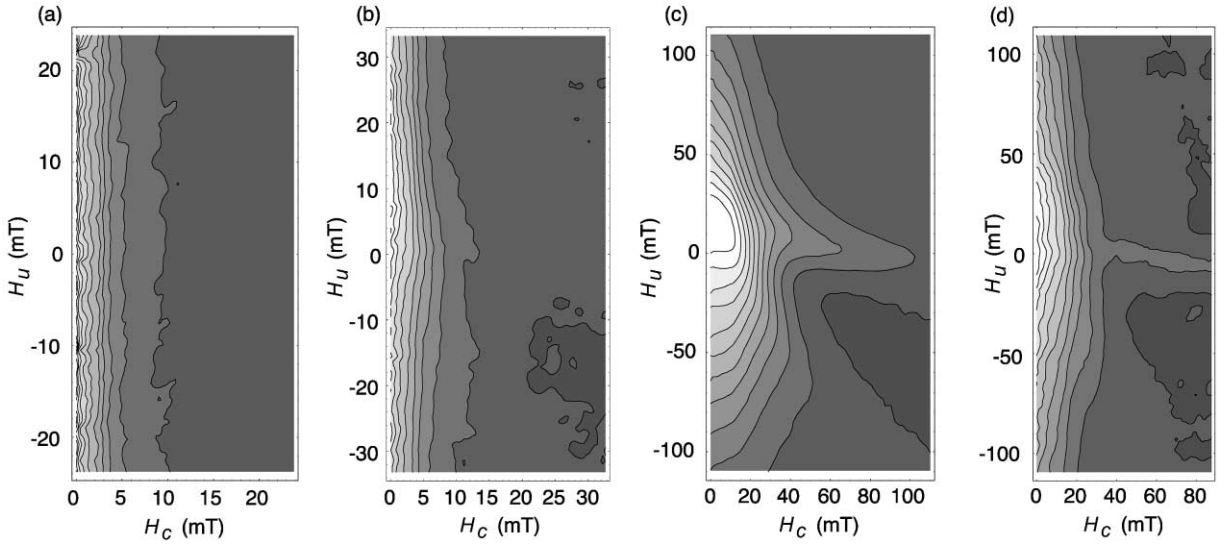

Fig. 6. FORC diagrams (SF = 3) for (a) a sample of M80 transformer steel; (b) a 2 mm grain of magnetite, after annealing; (c) the same 2 mm grain of magnetite before annealing; and (d) a 125 μm magnetite grain (no annealing) from sample HM4 (see Hartstra, 1982).

contour patterns have also been observed in Preisach diagrams for natural MD samples (e.g. Mullins and Tite, 1973; Ivanov et al., 1981; Ivanov and Sholpo, 1982; Zelinka et al., 1987; Hejda and Zelinka, 1990; Dunlop et al., 1990; Fabian and von Dobeneck, 1997). Roberts et al. (2000) showed, empirically, that natural samples located further in the MD direction on a Day plot (Day et al., 1977) have FORC distributions with larger degrees of divergence.

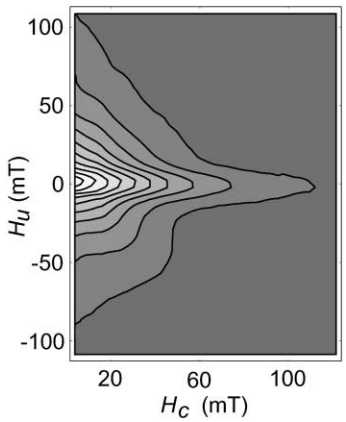

Fig. 7. FORC diagram (SF = 4) for an assemblage of MD particles in sample ODP 887B-2H-6-70 from the North Pacific Ocean (see Roberts et al., 1995).

The measured FORC diagram for our M80 transformer steel sample (Fig. 6(a)) is consistent with the analytical result of Bertotti et al. (1999a) for DW pinning with a WL process (Fig. 4(b)). That is, the diagram consists of vertical contours, with a FORC distribution function that decreases with increasing H_c. This result indicates that the simple classical model, although it is based on a dubious physical picture, somehow captures the physics of the hysteresis mechanisms in this sample. The FORC distribution for the 2 mm-sized magnetite grain after annealing (Fig. 6(b)) also has vertical contours consistent with those of the transformer steel and the result of Bertotti et al. (1999a). However, the FORC diagram for the 2 mm grain before annealing (Fig. 6(c)) is inconsistent with the result of Bertotti et al. (1999a) and the FORC diagram for the 125 μm magnetite (Fig. 6(d)) is intermediate between the results for the annealed and unannealed 2 mm magnetite sample. The inconsistency between the results for the annealed and unannealed samples implies that stress might be responsible for the deviation. Exactly how stress gives rise to this pattern is unknown. We suggest that in the annealed state, the pinning sites are homogeneously distributed throughout the sample in a manner that is consistent with a random process. In the unannealed state, however, with stress present, "pinning" might occur on

length scales comparable with the particle size. Thus, for example, stress might resist the movement of DWs from one end of the particle to the opposite end. In this case, the result of Bertotti et al. (1999a) would be inapplicable. It should also be noted that the results for the unannealed grain are highly asymmetrical about the central horizontal axis (Fig. 6(c)). This implies that the Preisach model is no longer a valid model of hysteresis for this sample, which also implies that the non-interacting one-dimensional classical DW model is no longer valid. It should also be noted that in Fig. 6(c) and (d) the darkest shadings indicate negative regions of the FORC distribution. This is also incompatible with the classical model. The results for our natural MD sediment sample (Fig. 7) are also not consistent with the Néel (1955) model in any obvious way.

5. Numerical DW pinning model calculations

In this section, we attempt to give the reader a more intuitive conceptual understanding for the result of Bertotti et al. (1999a) (i.e. that the classical DW pinning model predicts vertical lines on a FORC diagram). We also extend the (analytical) result of Bertotti et al. (1999a) with numerical calculations. Bertotti et al. (1999a) assumed that a pinning field can be represented by a WL process. Unfortunately, the WL process is not rigorously acceptable as a representation of the pinning field $H_p(x)$ for the following reason. If the values of a WL process are collected over a long interval of x, the result will not be a stable distribution of values. Instead, the spread of this distribution will increase with x, without limit (a random process with this property is referred to as a non-stationary process). Therefore, the WL process should be replaced with an Ornstein–Uhlenbeck (OU) random process, which is essentially a damped version of the WL process. Over a long enough interval of x, the collected values of an OU process will approach a limiting distribution with Gaussian form. This makes it acceptable as a model of $H_p(x)$. We therefore extend the model to an OU process. We note that Bertotti et al. (1999b) obtained an analytical expression for $\rho(h_c)$ in the case of an OU process, however, the solution is not in closed form and must be numerically solved. To our knowledge, this has not been done before. In addition, the solution of Bertotti et al. (1999a) neglects particle boundaries. We, therefore, incorporate particle boundaries into our calculations.

5.1. Sinusoidal DW energy

The mechanics of DW pinning hysteresis are easier to conceptualise if we begin by considering a sinusoidal DW energy. For the sake of simplicity, let A, M_s and $\mu_0 = 1$, so that Eq. (2) becomes

$$E_T(x, H) = E_w(x) - (L - 2x)H + \tfrac{1}{2}N(L - 2x)^2. \quad (5)$$

Next, let $E_w(x) = E_p/15\pi \cos[(L - x)(15\pi/2)]$ and $L = N = 1$ and $E_p = 1$. In Fig. 8(a), we show the resulting energy function $E_T(x, H)$ near $x = 0$ for several applied fields. At $H = 1.85$ (i.e. positive saturation), $E_T(x, H)$ has a positive slope everywhere. This implies that the DW is located at $x = 0$, or equivalently, it is annihilated; the magnetisation is positive everywhere. When H is ramped down to 0.95, a global minimum is still present at $x = 0$ on the left-hand side of the first pinning site; the stable low-energy state of the DW will therefore still be at $x = 0$. To the right of the first pinning site is a local minimum, which is a meta-stable location of the DW. When H is ramped down to 0.7, the minimum on the left-hand side of the first site is now only a local minimum (as opposed to a global minimum) and the DW is pinned here in a meta-stable location. When H is ramped down to 0.01, the minimum on the left-hand side of the first pinning site vanishes, and the DW makes a Barkhausen leap to the left-hand side of the second pinning site, which is still a local minimum. As the applied field H is decreased further on the major hysteresis loop, the DW will always be located at the minimum of $E_T(x, H)$ closest to $x = 0$. The location of the DW on the descending hysteresis loop will be denoted by $d_{HL}(H)$ and can be written as

$$d_{HL}(H) = \min[x : 0 \le x \le L : x \text{ is a local minimum of } E_T(x, H)]. \quad (6)$$

With this sinusoidal DW energy, the descending major hysteresis loop will have a Barkhausen leap for every maximum of $E_w(x)$.

On a FORC, when the applied field is increased from a reversal point H_a to a field H_b, the location of the DW will be denoted by $d_{FORC}(H_a, H_b)$. It can be shown that, on a FORC, the DW will be located

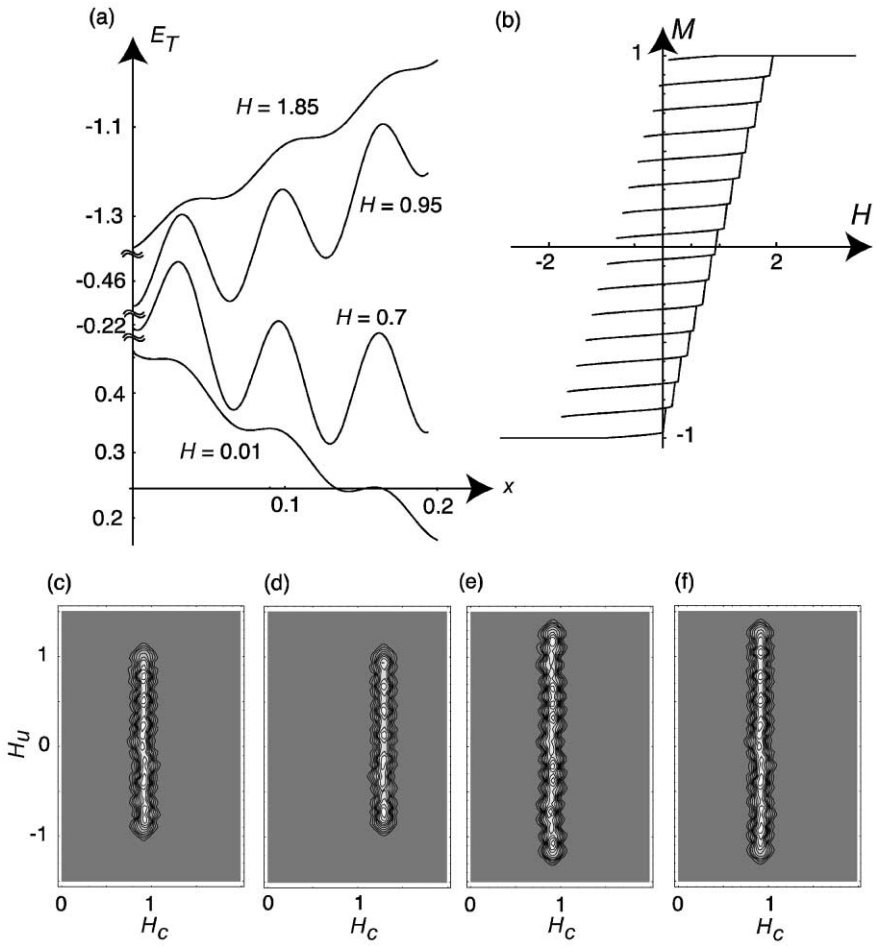

Fig. 8. (a) Total energy as a function of DW position x for various applied fields H calculated with sinusoidal DW energy in Eq. (5) for $E_p = L = N = 1$. The curly lines on the vertical axis represent breaks where the scale has been changed to emphasise the features on each curve. (b) A set of calculated FORCs for $E_p = L = N = 1$. Calculated FORC diagrams for (c) $E_p = L = N = 1$; (d) $E_p = 1.4$; (e) $N = 1.3$; and (f) $L = 1.3$.

at the minimum of E_T closest to, but less than, $x = d_{HL}(H_a)$. This can be written as

$$d_{FORC}(H_a, H_b) = \max[x : 0 \le x \le d_{HL}(H_a) : x \text{ is a local minimum of } E_T(x, H_b)]. \quad (7)$$

We used Eqs. (5)–(7), with $E_p = 1$ and $L = N = 1$, to calculate the FORCs in Fig. 8(b). Note that $E_w(x)$ has 15 peaks, or pinning sites, between $x = 0$ and 1. Consistent with this, the hysteresis behaviour in Fig. 8(b) can be decomposed into 15 hysterons. The demagnetisation field has horizontally spread these hysterons apart, so that each hysteron has a different bias. Similarly, in the resulting FORC diagram (Fig. 8(c)) there are 15 peaks present with an even vertical spacing (although not all the peaks are identifiable with the resolution of this diagram). Note that the pinning field is $H_p(x) = E_p \sin[(L/2 - x)15\pi]$ which has a maximum value of 1. The microcoercivity of the above-described hysterons is, to a good approximation, equal to this maximum pinning field. Hence, the peaks on the FORC diagram are all located at $H_c \approx 1$. The fact that the peak in Fig. 8(c) is located at slightly less than $H_c = 1$ is due to the fact that the pinning sites have widths of the same order as

L, and, hence, the demagnetisation field changes from one side of the pinning site to the other. If the width of the pinning sites was decreased, while keeping the maximum pinning field constant, then the distribution would approach $H_c = 1$ exactly.

When E_p is increased to 1.4 and the FORC diagram is recalculated (Fig. 8(d)), the microcoercivity of the peaks proportionately increases. When the demagnetisation constant N is increased to 1.3 (Fig. 8(e)), the vertical spread between peaks increases. When L is increased to 1.3 (Fig. 8(f)), the number of peaks increases but the spacing between peaks remains fixed. Hence, increasing the particle size and increasing N both give rise to a greater demagnetisation field and to greater vertical spread of the FORC distribution. However, increasing L also increases the number of pinning sites in a particle. The above treatment provides a simplified demonstration of how the parameters E_p, N, and L influence hysteresis behaviour and the resulting FORC diagram, in a simple one-dimensional DW pinning model.

5.2. The pinning field

In the previous section, we solved for $d_{HL}(H)$ by numerically locating the earliest local minimum of $E_T(x, H)$ with increasing x (see Eq. (6)). Alternatively, we can solve for $d_{HL}(H)$ by locating the earliest point, with increasing x, where the derivative of $E_T(x, H)$ is greater than zero. Hence, Eq. (6) can be rewritten as

$$d_{HL}(H) = \min\left[x : 0 \le x \le L : \frac{dE_T(x, H)}{dx} > 0\right]. \tag{8}$$

Similarly, Eq. (7) can be written as

$$d_{FORC}(H_a, H_b) = \max\left[x : 0 \le x \le d_{HL}(H_a) : \frac{dE_T(x, H)}{dx} < 0\right]. \tag{9}$$

At this point it is useful to rewrite Eq. (2) with the following scaled quantities: $h \equiv H/\mu_0 NAM_s$, $m \equiv M/AM_s$, $e_w \equiv E_w/\mu_0 A^2 NM_s^2$, and $e_t \equiv E_T/\mu_0 A^2 NM_s^2$. Then e_t becomes dimensionless:

$$e_t(x, h) = e_w(x) - hm + \tfrac{1}{2}m^2 = e_w(x) - h(L - 2x) + \tfrac{1}{2}(L - 2x)^2. \tag{10}$$

The derivative of $e_t(x, h)$ is

$$\frac{de_t(x, h)}{dx} = \frac{de_w(x)}{dx} + 2h - 2(L - 2x). \tag{11}$$

The scaled pinning field is denoted by $h_p(x) \equiv -(1/2)\, de_w(x, h)/dx$. Eqs. (8) and (9) can be rewritten as

$$d_{HL}(h) = \min[x : 0 \le x \le L : h > h_p(x) + (L - 2x)], \tag{12}$$

and

$$d_{FORC}(h_a, h_b) = \max[x : 0 \le x \le d_{HL}(h_a) : h < h_p(x) + (L - 2x)], \tag{13}$$

where $h_{de} \equiv -(1/2)de_{de}(x, h)/dx = (L - 2x)$ is the demagnetisation field. Hence, rather than working with the domain wall energy directly, we can work with its pinning field, which is the approach taken in most studies of DW pinning hysteresis (Néel, 1955; Dunlop and Özdemir, 1997; Bertotti, 1998).

Let us illustrate a simple method of graphically solving for $d_{HL}(h)$ and $d_{FORC}(h_a, h_b)$. In Fig. 9(a), we have plotted a hypothetical $e_w(x)$ for $0 \le x \le L$, where $L = 1$. In Fig. 9(b), we plot the sum of $e_w(x)$ and the demagnetisation energy, $e_{de} = (1 - 2x)^2/2$. In Fig. 9(c), we plot the pinning field $h_p(x)$. Note that the DW energy is made up of parabolic curves, so that its derivative (i.e. the pinning field) is made up of line segments. This form of $h_p(x)$ is referred to as a saw-tooth function (Néel, 1955). In Fig. 9(d), we plot the sum of $h_p(x)$ and the demagnetisation field, $h_{de} = (1 - 2x)$. The lower branch of the dashed curve in Fig. 9(d) illustrates the graphical solution of the upper major hysteresis loop, down to about $h = -1$. The upper branch of the dashed curve represents the solution of a FORC with reversal field at about -1. The vertical co-ordinate of this dashed curve is the applied field, h, while the horizontal co-ordinate is the position of the domain wall as a function of applied field. Where this dashed curve is horizontal, a Barkhausen leap occurs. Similar diagrams are found in Néel (1955) and Bertotti et al. (1999a).

A more detailed illustration of this graphical solution method is shown in Fig. 9(e), where we have expanded $h_p + h_{de}$ from Fig. 9(d) near $x = 0$. To solve Eq. (12) for the DW position on the upper major hysteresis loop, we need to find the earliest x such that $h \ge h_p + h_{de}$. For large h, this is just $x = 0$.

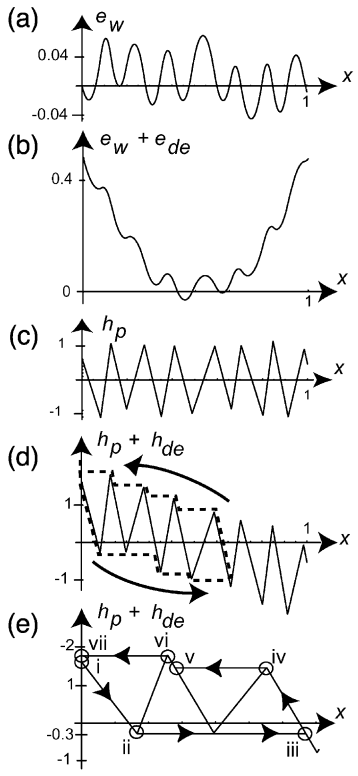

Fig. 9. (a) Hypothetical domain wall energy e_w for $x = 0$ to 1; (b) sum of e_w and the demagnetisation energy, e_{de}; (c) the pinning field h_p; (d) the sum of h_p and the demagnetisation field, h_{de}. The lower branch of the dashed line in (d) is a graphical solution of the DW location on the descending hysteresis loop, with a reversal field at about $h = -1$. The upper branch is a graphical solution of a FORC. A more detailed illustration of this graphical solution method is shown in (e), as described in the text.

Therefore, the domain wall is located at $x = 0$, and the magnetisation is positive everywhere. When h passes below about 1.6, the DW starts moving reversibly from points (i) to (ii), as labelled in Fig. 9(e). When h passes below about -0.3, the DW makes an irreversible Barkhausen leap from points (ii) to (iii), passing over a pinning site in between. Let us suppose that the applied field is reversed at about $h = -0.3$, and a FORC measurement is started. To solve Eq. (13) for the DW position on a FORC, we need to find the greatest x such that $h \leq h_p + h_{de}$ and such that the DW is to the left of its position at the reversal point. Hence, as h is increased from the reversal field (at about $h = -0.3$), the DW will travel reversibly from (iii) to (iv). Barkhausen leaps will then occur between (iv) and (v) and between (vi) and (vii). When the DW reaches (vii), the system will have reached positive saturation. Hence, a graphical solution of Eqs. (12) and (13) is obtained for the descending major hysteresis loop and for a FORC. This graphical solution method is useful for understanding the hysteresis behaviours of DW pinning described in the next section.

5.3. Random pinning function

Next, let us model h_p as an OU process. This is written as follows:

$$\frac{dh_p(x)}{dx} + \frac{h_p(x)}{\xi_h} = \frac{dW}{dx}, \tag{14}$$

where W is a WL process such that

$$dW = 0, \quad \langle |dW|^2 \rangle = \frac{2A_{h^2}\, dx}{\xi_h}, \tag{15}$$

and where ξ_h is a correlation length. The $h_p(x)/\xi_h$ term in Eq. (14) damps $h_p(x)$, resulting in a stationary process. Magni et al. (1999) showed that h_p generated by Eq. (14–15) has variance Ah_2.

To numerically generate $h_p(x)$ let us divide $x = \{0, L\}$ into N_L intervals. Let $h_p(i)$ represent the value of h_p at discrete points $x = i(L/N_L)$, where $0 \leq i \leq N_L$. Let us replace dW/dx in Eq. (14) on each interval with a constant value. We can treat these intervals as a type of correlation length $\xi_s \equiv L/N_L$ in the random term dW/dx of Eq. (14). Let the value of dW/dx on the ith interval be given by $R\Omega\sqrt{(2/\xi_s\xi_h)}$, where R is randomly selected from a normal distribution with mean zero and variance 1. It can be numerically shown that for ξ_s/ξ_h values much smaller than 1, the variance of $h_p(i)$ is approximated by Ω^2. Eq. (14) becomes

$$\frac{h_p(i+1) - h_p(i)}{(L/N_L)} + \frac{h_p(i)}{\xi_h} = R\Omega\sqrt{\frac{2}{\xi_s\xi_h}}, \tag{16}$$

or

$$h_p(i+1) = h_p(i)\left[1 - \frac{\xi_s}{\xi_h}\right] + R\Omega\sqrt{\frac{2\xi_s}{\xi_h}}, \tag{17}$$

where the initial condition $h_p(0)$ is randomly generated from the stationary distribution of $h_p(i)$. In Fig. 10(a)

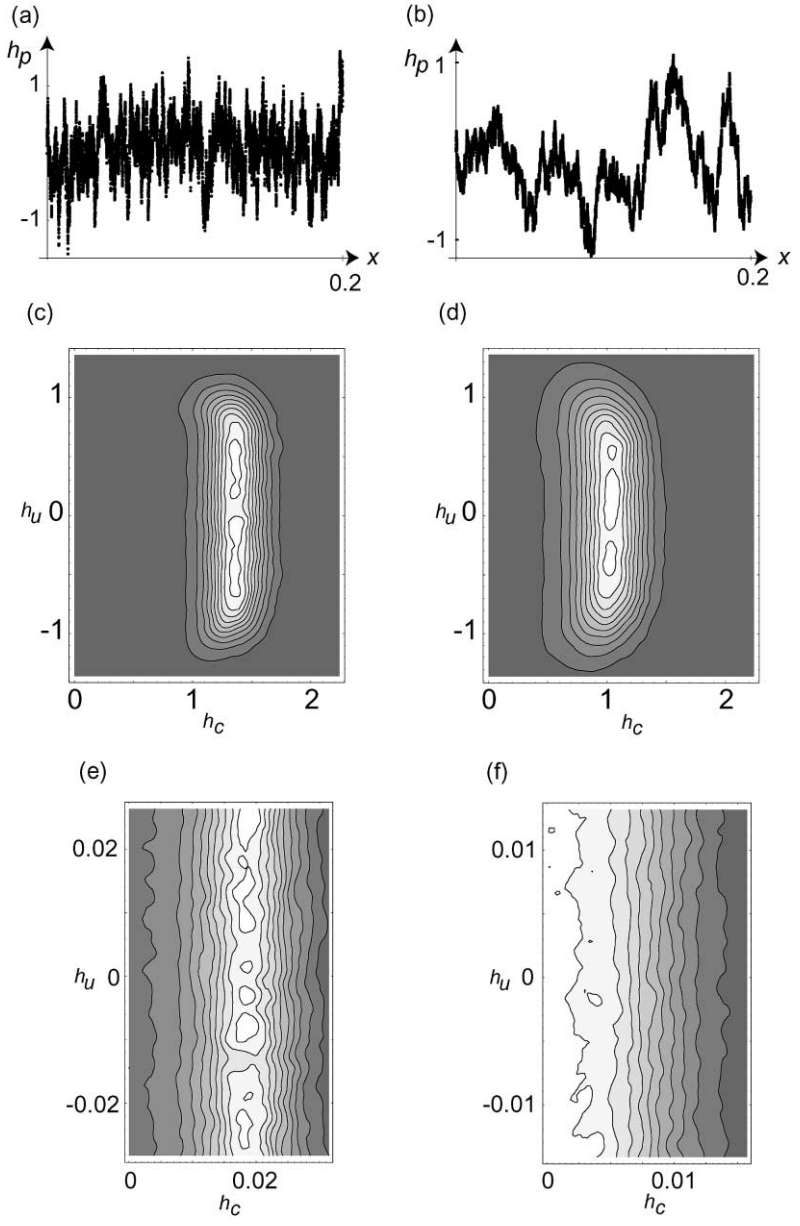

Fig. 10. Pinning field h_p for $x = 0$–0.2, generated using Eq. (17) with $i = 1$–20,000, where $x = i(L/N_L)$, $L = 1$, $N_L = 100{,}000$, $\Omega = 0.444064$ and (a) $\xi_s/\xi_h = 0.01$ and (b) $\xi_s/\xi_h = 0.001$. FORC diagrams calculated for: $\Omega = 0.444064$, (c) $\xi_s/\xi_h = 0.01$ and (d) $\xi_s/\xi_h = 0.001$. FORC diagrams calculated for: $\Omega = 0.0111016$, (e) $\xi_s/\xi_h = 0.01$ and (f) $\xi_s/\xi_h = 0.001$.

and (b), we plot h_p as a function of $x = i(L/N_L)$, for $i = 1$ to 20,000, $L = 1$, $N_L = 100{,}000$, $\Omega = 0.444064$, and $\xi_s/\xi_h = 0.01$ and 0.001, respectively. Although the two random functions have approximately the same variance, the function with larger ξ_s/ξ_h varies more rapidly (Fig. 10a and b).

In this discretized model, the DW location d becomes an integer between 0 and N_L; the magnetisation

becomes $m = L(1-(2d/N_L))$, and Eqs. (12) and (13) become

$$d_{\mathrm{HL}}(h) = \min\left\{ i : 0 \le i \le N_L : h \ge h_{\mathrm{p}}(i) + L\left[1 - \frac{2i}{N_L}\right]\right\}, \quad (18)$$

and

$$d_{\mathrm{FORC}}(h_{\mathrm{a}}, h_{\mathrm{b}}) = \max\{i : 0 \le i \le d_{\mathrm{HL}}(h_{\mathrm{a}}) : h \le h_{\mathrm{p}}(i) + L\left[1 - \frac{2i}{N_L}\right]\right\}. \quad (19)$$

FORCs and FORC diagrams were calculated for a distribution of grains. We first let $\Omega = 0.444064$, $N_L = 100,000$, $L = 1$, and $\xi_{\mathrm{s}}/\xi_{\mathrm{h}} = 0.01$. The resulting FORC distribution (Fig. 10(c)) is vertically elongated, which, as demonstrated by the sinusoidal model (Fig. 8(c)–(f)), is due to the demagnetisation field. The distribution is peaked at a microcoercivity of $h_{\mathrm{c}} = 1.4$, which we refer to as the dominant pinning field h_{dp}. The reason why the distribution is peaked at a dominant pinning field can be explained as follows. First, let us consider the case where there is no demagnetisation field, and only a random pinning field h_{p}, such as in Fig. 10(a). Suppose, the applied field is increasing and consider a DW that is pinned at a site with pinning field h_{p}^*. If the applied field continues to increase, and if the DW becomes unpinned from this site, then it will pass over all pinning sites with strength less than h_{p}^*, until it reaches a site with pinning field greater than or equal to h_{p}^*. Hence, as the DW moves, it will be pinned by progressively stronger pinning sites without limit. But, when we superimpose the random pinning field on the downward drift of a demagnetisation field h_{de}, as shown in Fig. 11, the above-described DW can be stopped by a field slightly weaker than h_{p}^*. Thus, as a DW moves with increasing field, it will initially be pinned at progressively stronger pinning sites, but this process will rapidly reach a limit and the strength of the pinning field will converge to a dominant pinning field. As the DW continues to move, pinning sites weaker than h_{dp} will be passed over by the DW, and sites stronger than h_{dp} will occur too infrequently to pin the wall over a statistically significant fraction of its movement. In effect, our treatment of the movement of a DW in the random pinning field shown in Fig. 10(a) can be simplified by keeping only sites with pinning strength close to h_{dp} or $-h_{\mathrm{dp}}$. On a FORC diagram, these pinning sites will give rise to hysterons with microcoercivity of h_{dp}. Hence, on a FORC diagram, the distribution will be peaked at $h_{\mathrm{c}} = h_{\mathrm{dp}}$.

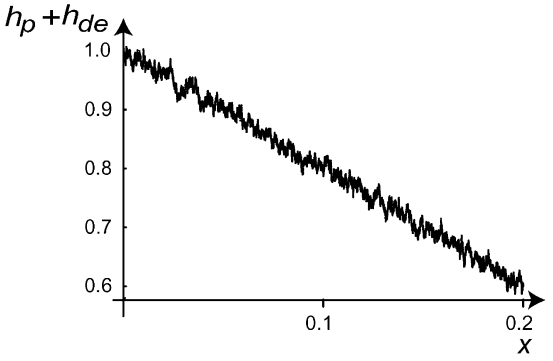

Fig. 11. Pinning field h_{p} summed with a demagnetisation field h_{de} for $x = 0$–0.2. The value of $h_{\mathrm{p}}(x)$ is generated using Eq. (17) with $i = 1$–20,000, where $x = i(L/N_L)$, $L = 1$, $N_L = 100,000$, $\Omega = 0.0111016$, and $\xi_{\mathrm{s}}/\xi_{\mathrm{h}} = 0.001$. The value of h_{de} is equal to $N(L - 2x)$ where $N = 1$.

When $\xi_{\mathrm{s}}/\xi_{\mathrm{h}}$ was decreased to 0.001 and the FORC diagram recalculated (Fig. 10(d)), we found that the dominant pinning field h_{dp} was reduced. This reduction can be explained as follows. A decrease in $\xi_{\mathrm{s}}/\xi_{\mathrm{h}}$ will cause h_{p} to vary more slowly (Fig. 10(b)). If the variation of h_{p} is slower, this means that when a DW becomes unpinned from a site with strength h_{p}^*, the probability that it will be stopped at a pinning site weaker than h_{p}^* is increased. Hence, the dominant pinning field will be reduced.

We next decreased the pinning field strength by decreasing Ω to 0.0111016, and recalculated the FORC diagrams for $\xi_{\mathrm{s}}/\xi_{\mathrm{h}} = 0.01$ and 0.001 (Fig. 10(e) and (f), respectively). The FORC distribution now has greater height than width, so we do not show the entire vertical extent of the distribution. As expected, a reduction in Ω causes a reduction in the dominant pinning field h_{dp} (compare Fig. 10(e) and (f) with (c) and (d), respectively). However, for $\xi_{\mathrm{s}}/\xi_{\mathrm{h}} = 0.001$, the FORC distribution appears to have become a decaying function for all values of h_{c} (Fig. 10(f)) in the neighbourhood of the origin. We argue that, in the limit of weak pinning fields and fixed $\xi_{\mathrm{s}}/\xi_{\mathrm{h}}$, the FORC distribution should approach a decreasing function for all h_{c}, consistent with the analytical result of Bertotti

et al. (1999a) (Eqs. (3) and (4)) for a WL process pinning field (Fig. 4(b)). The argument is that, with a weak pinning field, the idea of a dominant pinning field for an individual DW, as described above, loses its validity. But, we are considering a statistical distribution of DWs. Thus, by the same arguments made above, as the applied field is increased, a distribution of DWs will tend to become pinned by a stable statistical distribution of pinning strengths. In the limit of a weak pinning field, the DWs will reach this stable distribution after moving only a small distance. It can be shown from Eq. (14) that in the limit of small distances, the OU process is equivalent to a WL process. Hence, in the limit of a weak pinning field (and fixed ξ_s/ξ_h), pinning with an OU process pinning field becomes equivalent to pinning by a WL process field.

6. Discussion

Our numerical modelling demonstrates that a one-dimensional DW pinning model with an OU process pinning function and particle boundaries generates a FORC distribution with a vertically elongated peak, located at $h_c = p_d$, where p_d is the dominant pinning field. In the limit of weak pinning fields, p_d goes to zero (Fig. 10(f)) and the model becomes equivalent to the WL process studied by Bertotti et al. (1999a) (see Fig. 4(b)). The FORC distribution becomes a decreasing function of h_c only, with vertical contours in the neighbourhood of the origin (Fig. 10(f)). This result is consistent with experimental FORC diagrams for M80 transformer steel and for an annealed 2 mm magnetite grain (Fig. 6(a) and (b)) where DW pinning is dominant. However, this result is inconsistent with empirical FORC distributions for unannealed 2 mm magnetite and other natural MD particles (Figs. 6(c) and (d) and 7). We, therefore, conclude that the classical DW pinning model is inadequate for explaining hysteresis mechanisms in these MD samples.

The FORC distribution in Fig. 6(d) is highly elongated in the vertical direction. It might be possible to approximate this system, to first order, as a classical DW pinning system, with some additional mechanism present as a relatively small perturbation. The nature of this additional mechanism is not known; possibilities include DW nucleation and annihilation, DW interactions, and DW curvature. Whatever models might be proposed to describe hysteresis in MD particles, FORC diagrams will provide a sensitive test of their validity.

7. Conclusions

The classical DW pinning model, which was the starting point for this paper, is a highly simplified one-dimensional model of non-interacting planar DWs. We have shown that this model is consistent with hysteresis in bulk transformer steel and in annealed grains of magnetite on the scale of 2 mm. However, in our unannealed grains, where stress is present, the hysteresis behaviour is inconsistent with the classical model. The exact cause of this inconsistency is unknown: possibilities include DW nucleation and annihilation effects, DW interactions, and DW curvature.

We have used numerical calculations to extend the classical DW pinning model beyond the (analytical) result of Bertotti et al. (1999a), to include an OU process pinning function and grain boundaries. These extensions give us a better understanding of the classical model, but have not helped account for the unexplained hysteresis behaviours observed in our data. Furthermore, the fact that FORC diagrams for our unannealed samples are asymmetrical implies that the non-interacting one-dimensional classical DW model is not valid for such materials. It is therefore likely that a new model, which will probably also be phenomenological in nature, is needed to account for experimental data from many natural MD samples.

Acknowledgements

We are grateful to two anonymous reviewers and to Michel Prévot for constructive comments that helped to improve the paper. This work was supported by the University of Southampton Annual Grants Scheme, the Center for Statistics in Science and Technology at the University of California, Davis, and the US National Science Foundation (EAR-9909468).

References

Bertotti, G., 1998. Hysteresis in Magnetism. Academic Press, London.

Bertotti, G., Basso, V., Magni, A., 1999a. Stochastic dynamics in quenched-in disorder and hysteresis. J. Appl. Phys. 85, 4355–4357.

Bertotti, G., Mayergoyz, I.D., Basso, V., Magni, A., 1999b. Functional integration approach to hysteresis. Phys. Rev. E 60, 1428–1440.

Day, R., Fuller, M., Schmidt, V.A., 1977. Magnetic hysteresis properties of synthetic titanomagnetites. Phys. Earth Planet. Int. 13, 260–266.

Dunlop, D.J., Özdemir, Ö., 1997. Rock Magnetism: Fundamentals and Frontiers. Cambridge University Press, Cambridge.

Dunlop, D.J., Xu, S., 1994. Theory of partial thermoremanent magnetization in mulitdomain grains. Part 1. Repeated identical barriers to wall motion (single microcoercivity). J. Geophys. Res. 99, 9005–9023.

Dunlop, D.J., Westcott-Lewis, M.F., Bailey, M.E., 1990. Preisach diagrams and anhysteresis: do they measure interactions? Phys. Earth Planet. Int. 65, 62–77.

Eick, P.M., Schlinger, C.M., 1990. The use of magnetic susceptibility and its frequency dependence for delineation of a magnetic stratigraphy in ash-flow tuffs. Geophys. Res. Lett. 17, 783–786.

Everitt, C.W.F., 1962. Thermoremanent magnetisation. Part III. Theory of multidomain grains. Philos. Mag. 7, 599–616.

Fabian, K., von Dobeneck, T., 1997. Isothermal magnetization of samples with stable Preisach function: a survey of hysteresis, remanence, and rock magnetic parameters. J. Geophys. Res. 102, 17659–17677.

Halgedahl, S., Fuller, M., 1983. The dependence of magnetic domain structure upon magnetization state with emphasis upon nucleation as a mechanism for pseudo-single-domain behavior. J. Geophys. Res. 88, 6505–6522.

Hartstra, R.L., 1982. Grain-size dependence of initial susceptibility and saturation magnetization-related parameters of four natural magnetites in the PSD-MD range. Geophys. J. R. Astron. Soc. 71, 465–477.

Hejda, P., Zelinka, T., 1990. Modelling of hysteresis processes in magnetic rock samples using the Preisach diagram. Phys. Earth Planet. Int. 63, 32–40.

Ivanov, V.A., Sholpo, L.Y., 1982. Quantitative criteria for single- and multi-domain states in ferromagnetic minerals in rocks. Izvestiya Earth Phys. 18, 612–616.

Ivanov, V.A., Khaburzaniya, I.A., Sholpo, L.Y., 1981. Use of Preisach diagram for diagnosis of single- and multi-domain grains in rock samples. Izvestiya Earth Phys. 17, 36–43.

Magni, A., Beatrice, C., Durin, G., Bertotti, G., 1999. Stochastic model for magnetic hysteresis. J. Appl. Phys. 86, 3253–3261.

Mayergoyz, I.D., 1986. Mathematical models of hysteresis. IEEE Trans. Magn. MAG-22, 603–608.

McClelland, E., Sugiura, N., 1987. A kinematic model of TRM acquisition in multidomain magnetite. Phys. Earth Planet. Int. 46, 9–23.

Mullins, C.E., Tite, M.S., 1973. Preisach diagrams and magnetic viscosity phenomena for soils and synthetic assemblies of iron oxide grains. J. Geomag. Geoelectr. 25, 213–229.

Néel, L., 1955. Some theoretical aspects of rock magnetism. Adv. Phys. 4, 191–243.

Pike, C.R., Fernandez, A., 1999. An investigation of magnetic reversal in submicron-scale Co dots using first order reversal curve diagrams. J. Appl. Phys. 85, 6668–6676.

Pike, C.R., Roberts, A.P., Verosub, K.L., 1999. Characterizing interactions in fine magnetic particle systems using first order reversal curves. J. Appl. Phys. 85, 6660–6667.

Pike, C.R., Roberts, A.P., Verosub, K.L., 2001. FORC diagrams and thermal relaxation effects in magnetic particles. Geophys. J. Int. 145, 721–730.

Preisach, F., 1935. Über die magnetische Nachwirkung. Z. Phys. 94, 277–302.

Roberts, A.P., Pike, C.R., Verosub, K.L., 2000. FORC diagrams: a new tool for characterizing the magnetic properties of natural samples. J. Geophys. Res. 105, 28461–28475.

Roberts, A.P., Verosub, K.L., Weeks, R.J., Lehman, B., Laj, C., 1995. Mineral magnetic properties of middle and late Pleistocene sediments at ODP sites 883, 884 and 887, North Pacific Ocean. Proc. Ocean Drilling Prog. Sci. Res. 145, 483–490.

Shcherbakov, V.P., McClelland, E., Shcherbakova, V.V., 1993. A model of multidomain thermoremanent magnetization incorporating temperature-variable domain structure. J. Geophys. Res. 98, 6201–6216.

Schmidt, V.A., 1973. A multidomain model of thermoremanence. Earth Planet. Sci. Lett. 20, 440–446.

Worm, H.-U., 1999. Time-dependent IRM: a new technique for magnetic granulometry. Geophys. Res. Lett. 26, 2557–2560.

Zelinka, T., Hejda, P., Kropacek, V., 1987. The vibrating-sample magnetometer and Preisach diagram. Phys. Earth Planet. Int. 46, 241–246.